https://doi.org/10.5194/egusphere-2026-2448
Preprint. Discussion started: 5 May 2026

CO_2 Fertilization to Climate Limitation: Shifting Drivers in a Dryland Forest

Katja Irob[1], Liling Chang[2], Yakir Preisler[3], Sebastian Fiedler[4], Matthias Büchner[5], José M. Grünzweig[1], Efrat Sheffer[1]

1 - Institute of Plant Sciences and Genetics in Agriculture, The Robert H. Smith Faculty of Agriculture, Food and Environment, The Hebrew University of Jerusalem, Rehovot, Israel
2 - Department of Geography, Florida State University, Tallahassee, USA
3 - Agriculture Research Organization – Volcani Institute, Rishon LeZion Israel
4 - Department of Plant Ecology, Technische Universität Berlin, Berlin, Germany
5 - Potsdam Institute for Climate Impact Research, Member of the Leibniz Association, Potsdam, Germany

*Corresponding author: Katja Irob, katja.irob@mail.huji.ac.il

Abstract. Dryland forests represent a significant but uncertain component of the terrestrial carbon sink, where rising CO_2 and intensifying drought and heat stress exert opposing controls on carbon and water fluxes. Using ED2.2-hydraulics calibrated against 21 years of flux tower and inventory data from Yatir Forest, an arid pine plantation in Israel, we simulated carbon fluxes, biomass dynamics, and water-use efficiency under current climate and high-emission scenarios (SSP3-7.0, SSP5-8.5) through 2100 using five CMIP6 projections.

CO_2 fertilization initially enhanced productivity and biomass accumulation despite periodic drought, with the strongest response under SSP3-7.0. Under SSP5-8.5, compound heat and drought stress suppressed productivity below SSP3-7.0 levels despite higher CO_2 concentrations, triggering stand collapse in two projections and eliminating approximately 40% of accumulated biomass. GAM-based driver decomposition showed that forest responses shifted from CO_2-dominated to interaction-dominated by late century, with compound heat and drought stress explaining 25–63% of variance. Apparent biomass gains under severe scenarios reflected accumulation in fewer, larger surviving individuals as stand density declined, masking structural deterioration in aggregate metrics.

Functional decline (NEP, WUE) preceded structural changes by 12–37 years depending on scenario, providing an early warning window before visible deterioration. These results show that CO_2 fertilization benefits cannot compensate for the compound climate extremes that accompany high emissions, and that functional indicators must be monitored alongside structural metrics to detect forest vulnerability in dryland afforestation systems.

https://doi.org/10.5194/egusphere-2026-2448
Preprint. Discussion started: 5 May 2026

Keywords: afforestation, drought, legacy effects, Ecosystem Demography Model ED2.2, pine, compound stress, early warning signals, Yatir

1. Introduction

Under climate change dryland forests are shaped by two opposing forces: rising atmospheric CO_2, which can stimulate growth, and intensifying climate stress from warming and drought, which can suppress it (Peñuelas et al., 2017). Currently, terrestrial ecosystems absorb approximately 25–30% of anthropogenic CO_2 emissions, acting as a net carbon sink that takes up more CO_2 through photosynthesis and subsequent carbon storage in biomass and in the soil than they release via respiration and decomposition (Friedlingstein et al., 2022). Because of their vast extent and potential for carbon storage, dryland forests and dryland afforestation have been promoted as key climate mitigation tools (Yosef et al., 2018), although the extent and long-term stability of this carbon sink remain debated (Friedlingstein et al., 2019; Rohatyn et al., 2022). CO_2 fertilization plays a key role in sustaining the land carbon sink by increasing plant growth, carbon assimilation and water use efficiency, particularly when other resources are not limiting (Ruehr et al., 2023). However, whether the forest carbon sink will persist or shift toward becoming a carbon source depends on how these opposing drivers interact over time (Morán-Ordóñez et al., 2021), particularly under intensifying climate stress (Novick et al., 2016; Rohatyn et al., 2022).

Climate variability in dryland forests spans from severe droughts that challenge physiological thresholds to wet years that permit structural recovery (Klein et al., 2011). In dryland systems, elevated CO_2 can increase photosynthesis, improve intrinsic water-use efficiency, and prolong the period of positive carbon balance. However, these benefits are easily offset by water deficits and heat stress (Choat et al., 2018; Preisler et al., 2021). Furthermore, because dryland environmental variability dominates interannual fluctuations in carbon uptake (Ahlström et al., 2015), understanding the climatic drivers of drylands is critical for assessing the future of dryland carbon sink–source dynamics. For example, in the Mediterranean Basin, where precipitation limits productivity, climate change is shortening the cool, wet winters that define the growing season (Cos et al., 2022; Drori et al., 2021), increasing the risk for declines in forest productivity to the point that these forests may shift from carbon sinks to carbon sources.

Crucially, forest processes differ in both their sensitivity and response timescales to environmental change. Functional processes such as water uptake, gross primary productivity (GPP) and net ecosystem productivity (NEP) react rapidly, whereas changes in forest structure, such as biomass and leaf area, are buffered by internal tree reserves and allocation dynamics. Such differences can lead to responses at different timescales and magnitudes between forest function and structure, meaning that declines in water and carbon uptake may occur well before visible structural changes, or conversely, that structure may appear stable while function has already deteriorated (Preisler et al., 2021). These divergent response patterns are particularly evident during drought stress, which affects trees through multiple pathways operating across timescales.

https://doi.org/10.5194/egusphere-2026-2448
Preprint. Discussion started: 5 May 2026

Immediate drought responses include reduced photosynthesis and growth due to stomatal closure and declining leaf water potential (McDowell et al., 2008). Drought and high temperatures act synergistically, increasing vapor pressure deficits, whereas stomatal closure reduces evaporative cooling, further amplifying heat stress (Adams et al., 2009; Huang et al., 2024). If stress persists, physiological thresholds can be crossed, leading to hydraulic failure, reduced carbon available for growth due to increased allocation to tissue maintenance and repair, and canopy damage (Adams et al., 2009; Choat et al., 2018). These processes can drive sharp declines in NEP, sometimes shifting forests from net carbon sinks to sources and causing widespread mortality, as observed in the Mediterranean and other drought- or fire-prone regions (Dorman et al., 2015; Fatichi et al., 2019). Importantly, drought impacts extend beyond immediate responses: lagged mortality, reduced regeneration, and decomposition can prolong carbon losses for years (Anderegg et al., 2020; Reichstein et al., 2013). In already stressed systems, even moderate events can trigger long-term decline (Kannenberg et al., 2020; McDowell et al., 2020). Understanding these dynamics across multiple timescales, from immediate physiological responses to longer-term structural changes, is therefore essential to determine not only if forests will decline under climate change but also how and why.

Planted forests in climatically marginal regions, areas near the dry or thermal limits of forest viability, provide valuable test cases for understanding the temporal dynamics of ecosystem responses to multiple environmental drivers (Dorado-Liñán et al., 2019). Unlike natural forests, planted systems typically have well-documented histories, known tree ages, and simplified species compositions, allowing a clearer attribution of observed changes to specific environmental pressures. While empirical studies in dryland forests have advanced our understanding of short-term physiological forest responses to climatic events (Ogaya and Peñuelas, 2021; Väänänen et al., 2020), long-term, interacting feedbacks between CO_2, temperature, and water availability remain poorly understood. Moreover, in field settings environmental drivers co-vary, and experimentally isolating their individual and interactive effects across decadal timescales is impractical. Process-based models offer a complementary approach by explicitly representing physiological and structural processes and enabling mechanistic attribution of forest responses to environmental changes.

Here, we address this gap by using a process-based Ecosystem Demography Model (ED2.2-hydraulics; Xu et al., 2016; Longo et al., 2019) to examine how different functional and structural forest responses evolve under current and projected future climate scenarios (Chang et al., 2025). We focused on the well-equipped and well-monitored *Pinus halepensis* stand in the Yatir Forest, Israel (Grünzweig et al., 2003; Preisler et al., 2019). We first evaluated ED2.2-hydraulics' ability to reproduce observed fluxes and stand dynamics over two decades of monitoring, then used it to quantify the relative importance of CO_2 fertilization, water limitation, and heat stress as well as their interactions for stand dynamics and how these effects differ across time periods. Through this approach, we aim to identify the dominant environmental controls across timescales, assess when forest responses show signs of decline and which variables are most sensitive, and evaluate the long-term viability of dryland afforestation as a carbon sequestration strategy. Specifically, we asked: How does the relative contribution of climate stress and CO_2 fertilization to structural and functional forest responses shift over time under various climate change scenarios in a

https://doi.org/10.5194/egusphere-2026-2448
Preprint. Discussion started: 5 May 2026

dryland plantation? We hypothesized that CO_2 fertilization can partially offset climate-driven stress in the short term, but that increasing water and heat stress progressively constrain carbon uptake and structural stability over longer timescales.

2. Methods

2.1. Research Site

Our study focused on the Yatir Forest (31°20′N 35°03′E, 550–700 m elevation), a 2,800 hectare arid pine plantation established at the northern edge of the Negev Desert in Israel during the early 1960s. The forest has an average density of 300 trees ha^{-1} and is dominated by Aleppo pine (*Pinus halepensis* Mill.), a species widely regarded as being drought resilient and physiologically adapted to arid climates through traits such as efficient stomatal regulation and a deep rooting system. Yatir forest represents one of the largest and oldest afforestation projects in arid environments globally (Klein et al., 2014). The area has a Mediterranean-type climate (with precipitation concentrated in winter and spring, November–April), and is located within an arid zone (aridity index of 0.18; Rohatyn et al., 2023). It has a mean annual precipitation of 283 ± 84 mm and a mean annual temperature of 18.5 ± 0.5°C (2000–2020). The soils are predominantly light Rendzina (Haploxeroll), which is characterized by shallow depths and high carbonate contents. The forest is located at the climatic threshold for tree establishment making it an ideal case for examining how dryland forests respond to changing environmental conditions projected by future climate scenarios.

2.2. Ecosystem Demography Model ED2.2

We employed the Ecosystem Demography model version 2 (Longo et al., 2019; Moorcroft et al., 2001), a process-based terrestrial biosphere model that has been successfully applied to predict vegetation dynamics across diverse ecosystems, including Mediterranean forests and woodlands (Chang et al., 2025; Johnston, 2021) but with limited application in arid ecosystems. ED2.2 integrates cohort-level plant demography with spatial heterogeneity and ecosystem-scale biogeochemical processes, making it particularly suitable for examining forest responses to climate variability and extremes.

The model architecture combines several key components: (i) plant physiological processes, including photosynthesis, respiration, stomatal regulation, and carbon allocation; (ii) cohort-based demographic processes that track growth, mortality, and recruitment; (iii) canopy radiative transfer and energy balance calculations; (iv) soil–plant-atmosphere water and carbon fluxes; and (v) biogeochemical cycling of carbon. ED2.2 operates at hourly to daily time steps while tracking long-term ecosystem dynamics, enabling the simulation of both immediate physiological responses to weather and their cascading demographic consequences. A comprehensive model description is provided in Longo et al. (2019).

https://doi.org/10.5194/egusphere-2026-2448
Preprint. Discussion started: 5 May 2026

Specifically, we employed a version of ED2.2 that incorporates a trait-driven mechanistic plant hydraulic module, ED2.2-hydraulics (Xu et al., 2016), which explicitly simulates water transport through the soil–plant–atmosphere continuum and couples leaf water potential dynamics to both stomatal regulation and drought induced leaf shedding. The hydraulic framework tracks water flow based on tissue-specific conductance, accounts for xylem cavitation, and triggers leaf shedding when predawn leaf water potential falls below the turgor loss point, enabling more realistic simulation of plant responses to water stress than traditional empirical schemes (Xu et al., 2016), particularly in dryland areas.

Soil parameterization was based on (Klein et al., 2014) and Preisler et al. (2019) and included adjustments to the soil layer configuration, hydraulic properties (water retention and conductivity), texture, albedo, and rooting depth distribution. Furthermore, we adjusted the decomposition-specific soil moisture and temperature thresholds, along with the decomposition rates, to slow turnover to better represent arid conditions (Table S1).

2.3. Model Initialization

We initialized the model in two stages. First, we spun up ED2.2 from 1850 to 2014 using recycled historical climate and historical atmospheric CO_2 concentrations to equilibrate soil carbon pools. We extracted only the equilibrated soil carbon pools from this spin-up; all vegetation structure was discarded. Second, we initialized vegetation structure directly based on forest inventory measurements (individual tree height, diameter at breast height, species composition). The equilibrated soil carbon pools from the spin-up were then combined with the observed vegetation structure to initialize both the calibration simulations (2000-2020) and future projections (2015-2099). This approach ensured simulations began with observed forest structure while maintaining realistic soil carbon dynamics.

2.4. Model Parameterization and Calibration

We developed a *P. halepensis* Plant Functional Type (PFT) using western pine parameters from California's Sierra Nevada applications (Antonarakis et al., 2022; Chang et al., 2025) as a starting point. Plant functional types in ED2.2 are characterized by physiological, anatomical, and morphological parameters governing photosynthesis, respiration, hydraulic conductance, carbon allocation, and mortality thresholds.

We replaced the default parameters with *P. halepensis*-specific values (Table S1) through three approaches: (i) direct substitution with locally measured values, including: allometric relationships for DBH-height, DBH-aboveground biomass, DBH-LAI, DBH-root length, DBH-AGB (SI A3.2) as well as leaf structural traits and hydraulic properties, (ii) calibration within literature-informed ranges for parameters with observed variability but strong influence on model behavior (photosynthetic capacity, stomatal sensitivity, allocation fractions), and (iii) calibration for parameters without direct measurements but identified as influential through sensitivity analysis (cavitation thresholds, phenology triggers,

https://doi.org/10.5194/egusphere-2026-2448
Preprint. Discussion started: 5 May 2026

decomposition rates). All calibrated parameters were constrained within ranges informed by literature values and local ecosystem knowledge (detailed calibration description in Appendix A).

We first tuned soil hydraulic parameters to match observed soil moisture, then adjusted photosynthesis, stomatal regulation, phenology, and carbon allocation parameters to simultaneously match carbon fluxes, water fluxes, and growth trajectories. Parameter adjustments included soil and plant hydraulics, photosynthetic capacity, stomatal sensitivity, cavitation resistance, carbon allocation, leaf structural traits, and litter decomposition rates. These adjustments collectively transformed the model from a growth-maximizing temperate forest into a survival-optimized, water-limited forest model (details in Table S1).

Model evaluation used a 21-year dataset (2000–2020) that combines eddy covariance carbon and water fluxes, soil moisture records, and independent observations of the leaf area index (LAI, Sprintsin et al., 2011) and tree growth measurements from permanent plots.

2.5. Model Scenarios

We first evaluated model performance by simulating the observation period (2000–2020) against measured fluxes and stand characteristics at Yatir Forest (see Results, Section 3.1, SI A.2). Building on this validation, we simulated three climate scenarios from 2015–2099 to address our research question. The current climate serves as a baseline, representing climate conditions if present-day patterns persisted throughout the 21st century. This scenario was constructed by cycling the 21-year observed records (2000–2020) from Yatir Forest to generate the full 86-year simulation period.

For future climate projections, we used downscaled outputs from five general circulation models (GCMs, GFDL-ESM4, IPSL-CM6A-LR, MPI-ESM1-2-HR, MRI-ESM2-0, UKESM1-0-LL) under two contrasting shared socioeconomic pathways (IPCC, 2022): SSP3-7.0, a pathway with moderate-to-high greenhouse gas emissions; and SSP5-8.5, a fossil-fueled development pathway representing high emissions and the upper end of plausible radiative forcing by the end of the century. By using five GCMs for each SSP, we aimed to capture the uncertainty in climate projections. Hereafter, the term "scenario" refers to the ensemble of projections from the five climate models within each SSP pathway (SSP3-7.0, or SSP5-8.5) or their mean without additional repetitions.

2.5.1. Climate Input Data

We used bias-corrected climate projections from five CMIP6 general circulation models (GCMs) at 0.5° spatial resolution. These models were selected to represent a broad range of climate sensitivities and processed following the ISIMIP3b (Inter-Sectoral Impact Model Intercomparison Project, phase 3b) bias-correction protocol (Lange and Büchner, 2021). The ISIMIP3b protocol applies trend-preserving statistical bias correction to adjust systematic biases in the mean, variability, and distribution of climate variables in the GCM outputs relative to observations. The climate data were bias-corrected specifically for the Israeli grid via the ISIMIP3BASD v2.5 statistical bias adjustment and downscaling method. The daily meteorological variables included temperature, relative humidity, air pressure, wind speed, and global radiation and were associated with the

https://doi.org/10.5194/egusphere-2026-2448
Preprint. Discussion started: 5 May 2026

atmospheric CO_2 concentrations of the respective emission scenarios. Specific humidity $\boldsymbol{q}$ was calculated as a function of $\boldsymbol{e}$ (partial water pressure) and $\boldsymbol{P}$ (atmospheric pressure in Pascal) via the *humidity* R package (Cai, 2019).

For future precipitation (2015-2100), we used high-resolution daily re-analysis data (0.25°) from (Gebrechorkos et al., 2023) derived from the same five GCMs and SSP scenarios used in the ISIMIP3b dataset, which better captures seasonal dynamics critical for dryland systems. ISIMIP3b precipitation reproduced annual totals but showed spurious summer rainfall and distorted seasonal patterns. We therefore combined ISIMIP3b atmospheric forcing with Gebrechorkos et al. (2023) precipitation, applying bias correction (Appendix C2.1). All forcings were downscaled to hourly resolution to capture diurnal cycles and drought stress dynamics (Appendix C2).

2.5.2. Model Outputs and Variables Analyzed

We focused on a set of structural and functional response variables derived from the ED2.2 simulations and supported by site calibration. Structural variables included aboveground biomass (AGB), aboveground biomass growth rate, and leaf area index (LAI), which together characterize forest structure. Among these, AGB and average DBH capture long-term, cumulative growth, and the LAI and AGB growth rates reflect intermediate responses that adjust over seasons to years. Functional responses (net ecosystem productivity and water-use efficiency: WUE = GPP/Evapotranspiration) are rapidly-reacting flux-based processes that respond immediately to climatic variation and physiological regulation. Together, these response variables provide complementary perspectives on forest dynamics across short- to long-term timescales.

2.6. Statistical Analysis of Drought Trends and Forest Responses

To characterize projected drought dynamics under the different scenarios and their influence on forest responses, we quantified a drought severity index based on four stress indicators: (1) low precipitation (below the 20th percentile), (2) low soil moisture (below the 20th percentile), (3) extended dry season (dry months/year, <= 5 mm rain/month), and (4) high vapor pressure deficit (VPD; above the 80th percentile), representing atmospheric drought (Shekhar et al., 2024). Each indicator was binary (present or absent), and the composite index ranged from 0 (no drought) to 4 (extreme compound drought).

For the current climate scenario (2015-2100), we recycled the 21-year observational period (2000-2020) by randomly sampling years without replacement in successive 21-year blocks. This approach preserved realistic climate variability while avoiding artificial persistence of specific drought sequences. Consequently, precipitation patterns repeat every 21 years (as a direct climate forcing), but soil moisture, dry season length, and VPD reflect lagged and integrated responses that differ across cycles due to antecedent conditions and ecosystem state. For future scenarios (SSP3-7.0, SSP5-8.5), we calculated the annual proportion of models ($N = 5$ GCMs) experiencing each stress indicator and visualized ensemble-mean contributions through 2100.

https://doi.org/10.5194/egusphere-2026-2448
Preprint. Discussion started: 5 May 2026

Probability density functions (PDFs) and summary statistics were computed for each climate scenario across three temporal periods (early: 2015-2040, mid: 2041-2070, late: 2071-2099), including the percentage of years with severe (drought severity = 3) or extreme (drought severity = 4) drought severity. Temporal changes within scenarios were assessed via Kruskal–Wallis tests to compare drought severity distributions between temporal periods. Between-scenario differences were evaluated via Kruskal–Wallis tests for drought severity distributions and chi–square tests for drought component dominance patterns. When significant differences were detected ($p < 0.05$), Dunn's tests with Bonferroni correction were applied for post hoc pairwise comparisons ($N = 5$ GCMs). All analyses were performed via R software, version 4.5.1 (R Core Team, 2025).

2.6.1. Projected Drought Severity

The projected climate trajectories consistently indicate more frequent and severe droughts throughout the 21st century, particularly under SSP3-7.0 and SSP5-8.5 (Figs. 1, S14; Table S4). While the mean annual precipitation (MAP) generally decreased, SSP5-8.5 is characterized by heightened variability, with both extremely dry and wet years becoming more common. Ensemble averaging across GCMs compresses this variability; individual projections show more severe precipitation deficits than the mean representation suggests. Drought years (<200 mm, roughly corresponding to the 20th percentile of the current climate distribution) are projected to increase from ~7% under the current climate to 20–34% by the late century, with severe droughts (<150 mm, ~10th percentile) tripling in frequency. In addition, the rainy season is several weeks shorter, and increasing evaporative demand further exacerbates aridity (Fig. 1).

Our multicomponent drought severity analysis revealed a fundamental shift in drought type under climate change. While current climate conditions showed stable drought patterns over time (trend test $p > 0.05$), both SSP3-7.0 and SSP5-8.5 exhibited significant temporal intensification ($p < 0.01$), with severe drought frequency doubling under SSP3-7.0 and increasing 6.7-fold under SSP5-8.5. Critically, SSP5-8.5 was distinguished by a complete compositional shift toward VPD-dominated drought events (occurring in 99.8% of the years), indicating that atmospheric demand became the primary drought driver rather than a precipitation deficit. Full statistical comparisons across models and scenarios, including drought severity distributions and changes in rainy season length, are provided in the supporting material (Appendix C).

https://doi.org/10.5194/egusphere-2026-2448
Preprint. Discussion started: 5 May 2026

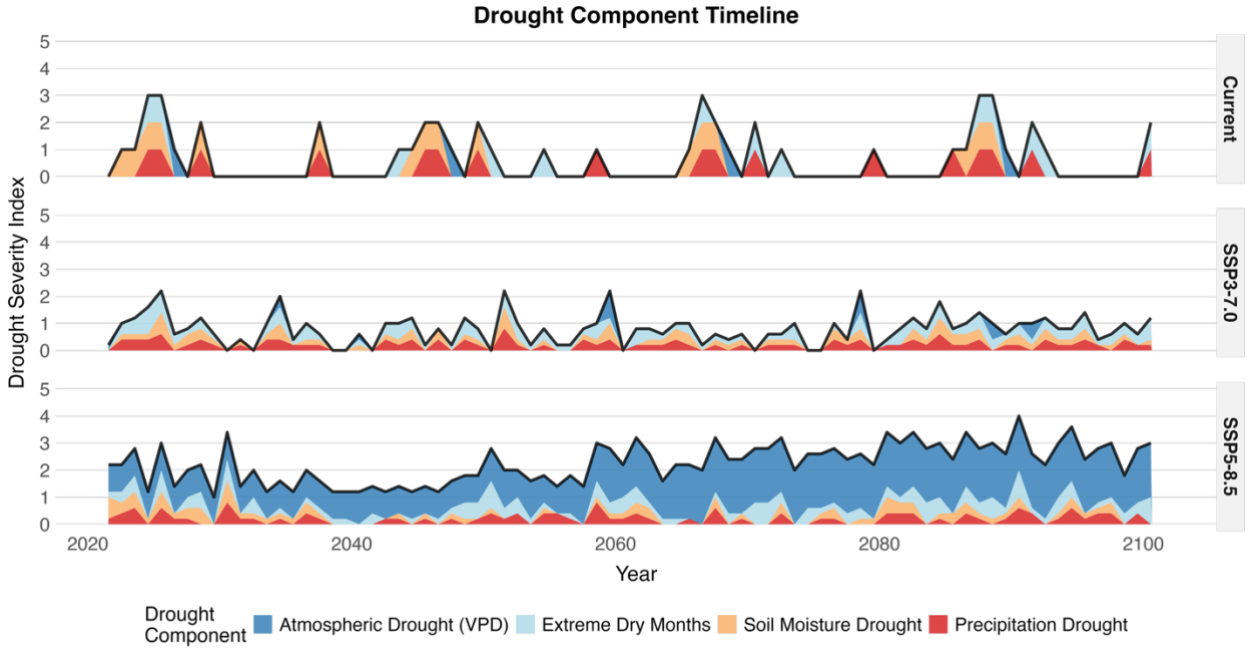

Figure 1: Temporal composition of compound drought events averaged per climate scenario, showing the relative contributions of four key stress indicators: high atmospheric demand (warming-induced VPD), extremely dry months, low soil moisture, and low precipitation. Drought components represent ensemble means across 5 GCMs for each SSP scenario, smoothing individual model drought events, whereas Current represents a single observed climate sequence.

2.6.2. Early Warning Signal Analysis

We quantified temporal lags between forest functional decline and structural change to identify early warning indicators of ecosystem stress (Table S2). For functional variables (NEP, WUE) and structural growth rates (AGB growth, LAI), we detected decline onset as the first year when 15-year rolling mean trends showed significant negative slopes ($p < 0.1$, slope thresholds: -0.002 yr^{-1} for NEP and WUE, -0.001 yr^{-1} for AGB growth, -0.005 yr^{-1} for LAI). For cumulative structural variables (total AGB, mean DBH), we detected growth stagnation when 15-year rolling relative growth rates fell below 0.5% yr^{-1} for AGB and 0.2% yr^{-1} for DBH. Analysis began in 2030 to exclude model spin-up artifacts.

Time lags were calculated as the number of years passed between the onset of functional decline (earliest of NEP or WUE decline) and the onset of structural stagnation. We computed mean lags and standard deviations across models within each scenario.

https://doi.org/10.5194/egusphere-2026-2448
Preprint. Discussion started: 5 May 2026

2.6.3. Environmental Driver Analysis

To quantify the relative influence of environmental drivers on forest structural (DBH, AGB, AGB growth rate, LAI) and functional (NEP, WUE) responses, and to assess how driver importance and their interactions differ across time periods, we used generalized additive models (GAMs) with tensor product interactions (Wood, 2017). The analyses were based on annual summaries of simulated outputs, aggregated by hydrological year (October–September), with seasonal metrics calculated where relevant. The analysis exploits the quasi-factorial structure inherent in the simulation design: two emission scenarios provide different CO_2 trajectories, multiple GCMs generate climate variability within each scenario, and current climate runs isolate CO_2 effects from climate change, together creating spread across driver combinations without requiring controlled manipulation.

For each response variable, we fitted separate GAM models for three temporal periods (early: 2015–2040; mid: 2041–2070; late: 2071–2099) to capture the evolving relationships between environmental drivers and forest responses. Each model included smooth terms for nine environmental predictors (CO_2 concentration, mean annual temperature, number of heat stress months (Temp > 3rd quartile), mean soil moisture, dry season soil moisture, wet season soil moisture, total annual precipitation, ET/P ratio, and mean annual VPD), plus tensor product interaction terms (ti) for seven key driver combinations (CO_2 × soil moisture, CO_2 × ET/P, heat stress × dry season soil moisture, temperature × precipitation, precipitation × ET/P, CO_2 × VPD, CO_2 × dry season soil moisture). We used the bam function from the *mgcv* package (Wood, 2017) with fast restricted maximum likelihood (fREML) estimation and automatic shrinkage of non-significant terms. To account for temporal autocorrelation within each GCM-scenario run, we specified a first-order autoregressive (AR1) residual correlation structure ($\rho = 0.3$) grouped by simulation run. Variance explained by each driver or interaction was calculated as the proportion of the total penalized F-statistic × degrees of freedom, providing a measure of relative importance that does not depend on predictor scale or range. To facilitate comparison across response variables and periods, we grouped individual drivers into three categories based on their physiological effects: CO_2 fertilization (CO_2), water limitation (all soil moisture and precipitation metrics), and temperature/atmospheric stress (temperature, heat stress months, VPD). We report the summed variance explained by drivers within each group and by all significant interactions ($p < 0.05$).

3. Results

We first present the results of the Model Calibration, then we show the resulting ecosystem dynamics simulated by our calibrated model for the Yatir Forest under three scenarios, with a focus on (i) structural and functional forest responses, (ii) early warning signals of functional decline and (iii) the relative importance and temporal transition of environmental drivers.

3.1. Model Evaluation and Fit

https://doi.org/10.5194/egusphere-2026-2448
Preprint. Discussion started: 5 May 2026

Model evaluation used a 21-year dataset (2000–2020) that combines eddy covariance carbon and water fluxes, soil moisture records, and independent observations of the leaf area index (Sprintsin et al., 2011) and tree growth. The full evaluation metrics (RMSE, R^2, and bias) and data sources are provided in Appendix A2.

The parameter combination that achieved the best overall fit (composite score 88.3%; Appendix A2) showed strong agreement for vegetation structure (LAI: 86.6%, Fig. 2a), soil moisture (91.2%; Fig. 2b), and evapotranspiration (91.3%, Fig. S1). Among the carbon fluxes (Fig. S2), model–data agreement was strongest for gross primary productivity (GPP; 89.3%, Fig. 2c) followed by net primary productivity (NPP; 85.6%, Fig. S2) and net ecosystem productivity (80.6%, Fig. 2d). The best calibrated model underestimated the spring peak in carbon fluxes (Fig. 2c,d), likely due to fixed physiological parameters that cannot reproduce the sharp response of Aleppo pine physiology when all environmental constraints are simultaneously relaxed (see Discussion). Independent validation against dendrometer measurements (Klein et al., unpublished data) confirms realistic DBH growth rates (simulated: 4.5 mm/year vs. observed 5.0 mm/year; Fig. S3). Overall, the calibrated model reproduced the seasonal cycles and drought–response patterns characteristic of the Yatir Forest, indicating robust performance across both structural and functional responses.

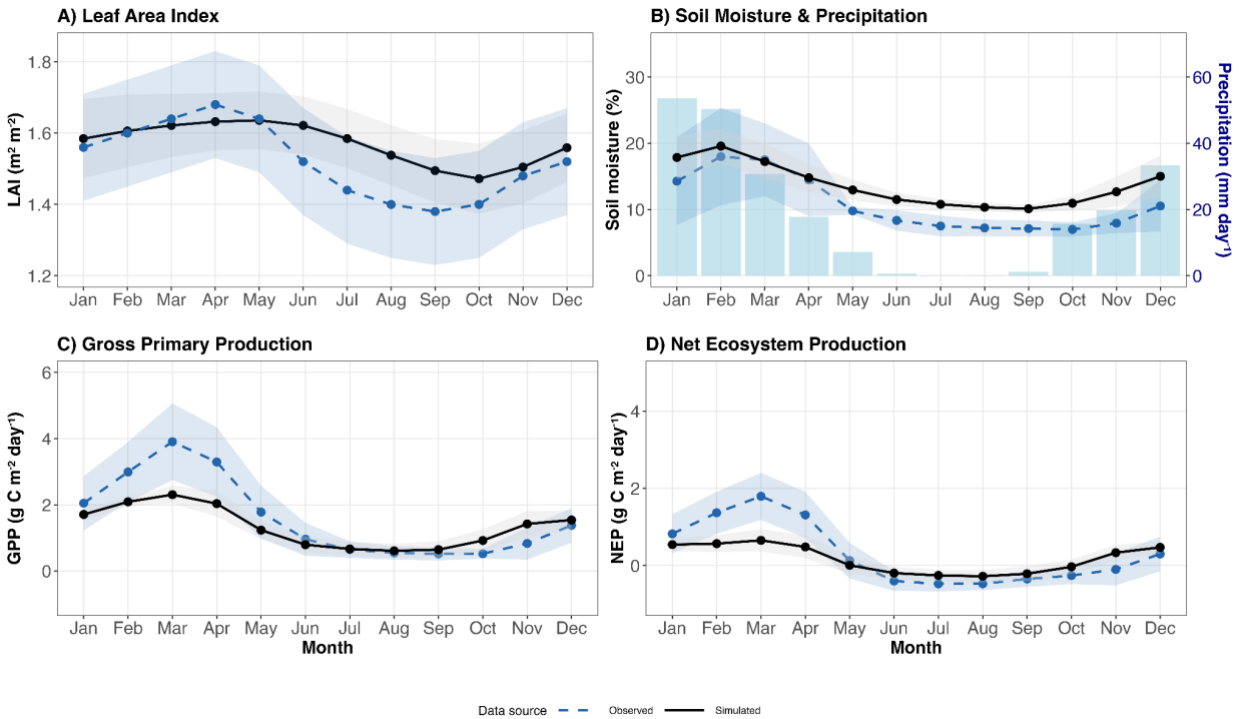

Figure 2: Comparison of simulated and observed mean seasonal dynamics of leaf area index (a), soil moisture (b), GPP (c) and NEP (d) at Yatir Forest, averaged monthly over 21 years (2000-2021), to characterize the typical seasonal pattern critical to dryland forest function. Lines show monthly means (black = simulation, dashed blue = observations) and ribbons show the

https://doi.org/10.5194/egusphere-2026-2448
Preprint. Discussion started: 5 May 2026

interannual variability (±1 SD across years). In b) monthly mean soil water content plotted alongside mean monthly precipitation (bars, right axis).

3.2. Forest Response

3.2.1. Structural Responses Show Early Increase and Late-century Divergence Under High Emissions

The future climate reshaped forest structure but in different directions and magnitudes depending on the response variable. Mean DBH increased steadily under all scenarios, with the greatest increase occurring under high-emission scenarios (SSP5-8.5, SSP3-7.0) reaching 70-80 cm by 2100, while under current conditions DBH only increased to near 40 cm (Fig. 3a.1). Rising mean DBH reflected survivor bias and persistent recruitment bottleneck rather than enhanced growth: as smaller cohorts grew into larger size classes or died without replacement, the population mean shifted towards fewer, larger trees (Fig. S4). However, two of five SSP5-8.5 projections (gfdl-esm4, mpi-esm1-2-hr) experienced abrupt stand-level collapse, with mean DBH dropping ~30 cm within a single month (see the sharp drop of two lines around 2080 in Fig. 3a.1). In these projections, CO_2-driven biomass accumulation had produced the largest trees (AGB exceeding 5 kg C/m², Fig. 3a.2), whose stem maintenance respiration costs exceeded carbon assimilation (Fig. S8), creating persistently negative carbon balance that triggered mortality. Mortality events triggered site-level structural reorganization, coinciding with AGB losses (Fig. 3a.2) and LAI redistribution (Fig. 3a.4).

For AGB, SSP3-7.0 showed the strongest accumulation, reaching 5-8 kg C/m² by 2100 (Fig. 3a.2). SSP5-8.5 accumulated less biomass than SSP3-7.0 throughout the simulation and remained comparable to or below Current climate levels for most projections, reflecting the earlier onset of climate limitation under more severe warming and drought. Two SSP5-8.5 projections experienced abrupt AGB losses coinciding with the stand-level collapse described above, dropping from >5 to ~3 kg C/m² (Fig. 3a.1). Current climate showed slow, steady accumulation plateauing around 3 kg C/m² through 2100 (Fig. 3a.2). Continued AGB accumulation, despite declining stem density (Fig. S6) and increasing mortality (Fig. S7), reflected the nonlinear scaling of wood biomass with diameter: per-tree biomass gains temporarily outpaced losses from tree mortality and consequential decomposition. AGB growth rates remained highly variable, with high-emission scenarios showing higher but unstable rates and current climate showing lower rates and even zero growth in dry years (Fig. 3a.3).

LAI patterns revealed different climate constraint mechanisms (Fig. 3a.4). Current climate maintained stable LAI (~1.5-2.0) throughout most of the century with slight declines in the last decades. The SSP3-7.0 scenario initially supported higher LAI (~1.7-2.5) through mid-century but later showed decline in all model projections, falling to levels comparable to or below Current climate. SSP5-8.5 showed the lowest LAI for most of the simulation period (~1.1-1.7). Some of its projections showed episodic spikes after 2080, coinciding with AGB losses (Fig. 3a.2).

https://doi.org/10.5194/egusphere-2026-2448
Preprint. Discussion started: 5 May 2026

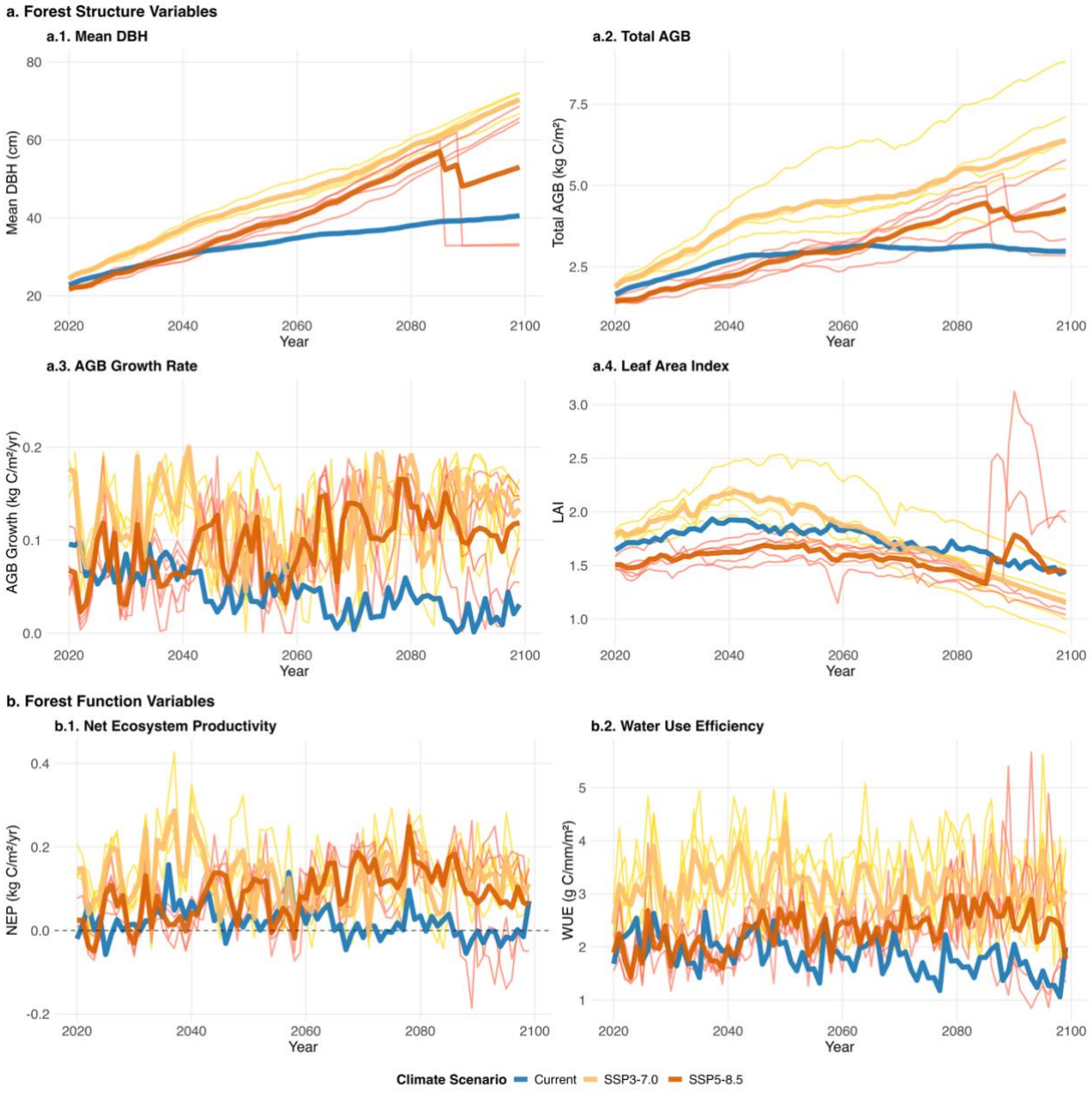

Figure 3: Time series of key structural and functional responses of a dryland pine forest 2020-2100 under current (blue), and two high emission scenarios, SSP3-7.0- (light orange), and SSP5-8.5 (dark orange) scenarios. Thick lines represent the mean of five models per scenario (thin lines). a: Simulated temporal trajectories of forest structural responses under different climate scenarios: (a.1.) mean diameter at breast height (DBH), (a.2.) aboveground biomass (AGB), (a.3.) AGB growth rate and (a.4.) leaf area index (LAI). b: Simulated temporal trajectories of forest functional responses under different climate scenarios: (b.1.) net ecosystem productivity (NEP) and (b.2.) water use efficiency (WUE).

https://doi.org/10.5194/egusphere-2026-2448
Preprint. Discussion started: 5 May 2026

3.2.2. Productivity Increases with CO_2 Fertilization but Destabilizes with Drought

Net ecosystem productivity diverged sharply by scenario, but also by GCM within each scenario. Current climate NEP oscillated frequently between carbon source and sink throughout the century, with many years showing negative NEP, indicating that without CO_2 fertilization the forest operates near carbon neutrality (Fig. 3b.1). Both high emission scenarios showed higher mean NEP than Current climate, but individual projections frequently crossed into negative values throughout the century, reflecting the high interannual sensitivity to drought conditions. SSP3-7.0 showed the highest mean productivity early in the century, while SSP5-8.5 mean NEP exceeded SSP3-7.0 by late century despite more severe climate conditions, likely reflecting sustained CO_2 fertilization benefits for fewer surviving trees under reduced competition. SSP5-8.5 showed the greatest interannual variability, with individual projections spanning from strongly positive to negative NEP in consecutive years. The two projections that experienced stand-level dieback (Figs. 3a.1, 3a.2) showed corresponding sharp NEP declines.

Water-use efficiency showed clear scenario separation (Fig. 3b.2). SSP3-7.0 exhibited the highest WUE, increasing steadily through the century as CO_2-driven stomatal regulation improved carbon gain per unit water transpired. SSP5-8.5 showed moderate WUE increases with high interannual variability; two projections displayed sharp late-century spikes as a result of the stand-level dieback events described above. Current climate maintained the lowest WUE (~1.5-2.0 g C/mm/m²) with a slight decline in the final decades.

3.3. Early Warning Signals

We identified the onset of sustained decline (negative 15-year rolling trend, $p < 0.1$) for each response variable across climate scenarios (Tables S2a,b). Under SSP3-7.0, functional decline (NEP or WUE) and AGB growth rate stagnation occurred simultaneously in all five models (mean onset 2037 ± 0). LAI declined 2 ± 3 years later (mean onset 2039 ± 3). However, biomass stagnation followed 18 ± 6 years after the onset of functional decline (range: 12–25 years, mean onset 2055 ± 6), occurring in all five models by 2099. Under SSP5-8.5, decline onset was later and more variable across models. WUE declined earliest (mean onset 2041 ± 10, 4/5 models), followed by AGB growth rate (2048 ± 16, 4/5 models), LAI (2049 ± 7, 5/5 models), and NEP (2053 ± 16, 3/5 models). Biomass stagnation occurred in only 2 of 5 models, with a mean warning window of 22 ± 21 years after functional decline (range: 7–37 years, mean onset 2067 ± 21).

3.4. Driver Shifts from Fertilization to Drought Stress

To identify the dominant environmental controls of forest structure and function, we analyzed driver importance across all climate scenarios and models via GAM-based variance decomposition across all climate scenarios and models (Fig. 4; Tables S3, S4).

https://doi.org/10.5194/egusphere-2026-2448
Preprint. Discussion started: 5 May 2026

In the early century period (2015–2040), individual drivers explained the majority of variance across all response variables (72–93%; Fig. 4a; Table S3), with interactive effects contributing 7–27% (Table S4). CO_2 was the dominant individual driver for mean DBH (85%) and total AGB (76%; Fig. 4b), while water stress dominated AGB growth (49%), NEP (41%) and WUE (39%). Temperature and VPD stress combined explained substantial early-century variance for LAI (46%) and NEP (41%) but tended to decline in importance along the century for most variables. Interaction effects were small in this period, but CO_2 × VPD was the most consistent, explaining only 2–8% of variance across most variables, while CO_2 × dry season soil moisture contributed to NEP (5%) and AGB (3%) (Table S4).

By mid-century (2041–2070), individual drivers remained dominant across most variables (66-95%; Fig. 4a, Table S3), with interactive effects increasing notably only for LAI (34%) and AGB (26%). Among individual drivers, CO_2 remained dominant for DBH (83%) but declined for AGB (40%). Water stress became the dominant individual driver for WUE (67%), AGB growth (65%), and NEP (49%). The most prominent interactions were CO_2 × VPD for LAI (13%), heat stress × dry season soil moisture for AGB (10%), and temperature × precipitation for NEP (10%) (Table S4).

By late century (2071–2099), interactive effects accounted for 39–55% of variance in structural variables and 60–66% in functional variables (Fig. 4a, Table S3), reflecting increasingly non-additive responses to combined environmental forcing. Among individual drivers, CO_2 effects weakened for most structural variables (DBH: 32%, AGB: 26%) and became non-significant for NEP and WUE in isolation. Water stress maintained consistent importance for AGB growth (55%), WUE (32%), and LAI (32%). The dominant interactions intensified: heat stress × dry season soil moisture explained 11–25% of variance across variables (up to 25% for AGB), while temperature × precipitation explained 12–21% (up to 21% for WUE). For NEP, CO_2 × dry season soil moisture interactions became prominent (20%) (Table S4).

https://doi.org/10.5194/egusphere-2026-2448
Preprint. Discussion started: 5 May 2026

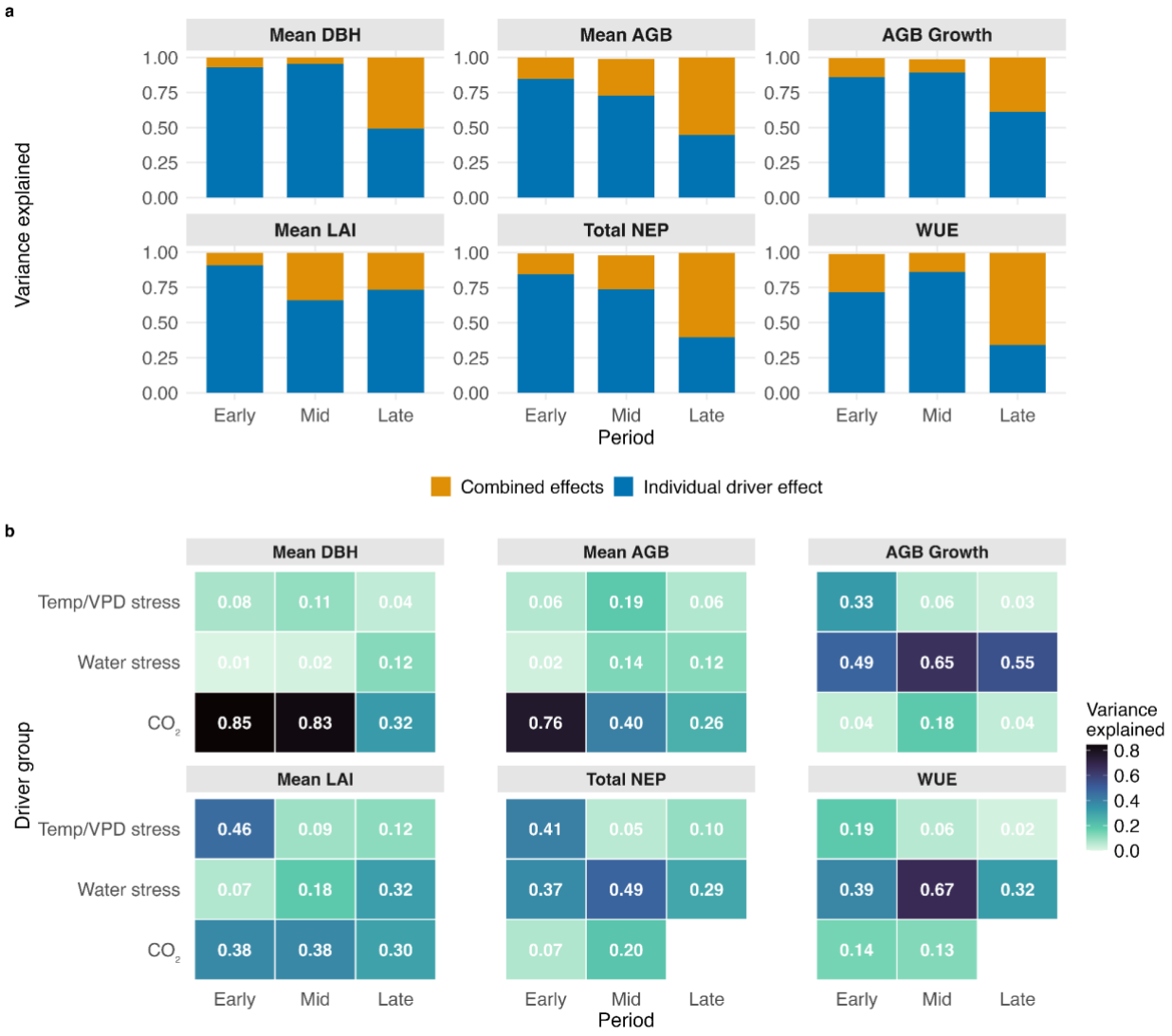

Figure 4: Temporal evolution of environmental driver effects. (a) Proportion of total variance explained by individual driver effects (blue) versus combined interactive effects (orange) across three time periods in the simulations (early: 2015–2040, mid: 2041–2070, late: 2071–2099) for the response of structural (mean DBH, total AGB, AGB growth rate, LAI) and functional (NEP, WUE) forest variables. (b) Heatmap of variance explained by grouped drivers across response variables and time periods. Environmental drivers are grouped into CO_2 fertilization, water stress, and temperature/VPD stress categories. Cell values indicate the summed variance explained by all significant individual drivers ($p < 0.05$) within each group. Missing cells indicate no significant effects. Darker colors represent greater variance explained.

https://doi.org/10.5194/egusphere-2026-2448
Preprint. Discussion started: 5 May 2026

4. Discussion

We investigated how climate change affects forest structure and function in a planted dryland pine forest, focusing on the interactive effects of elevated CO_2, water limitation, and warming over time. Our findings offer new insights into (i) the temporal evolution of dominant environmental drivers, including the transition from CO_2 fertilization to climate limitation; (ii) the differential responses of forest structure and function; and (iii) the implications for monitoring, afforestation, and forest management.

4.1. Temporal Transitions in Environmental Drivers

CO_2 fertilization benefits in dryland forests depend on climate conditions and forest state. Early century, CO_2 enrichment increased photosynthesis and water-use efficiency, driving increases in net ecosystem productivity and biomass accumulation (Fig. 3). As conditions became warmer and drier, with higher VPD and reduced soil moisture (Fig. 1), CO_2 benefits saturated and water availability increasingly constrained productivity.

Under current climate with constant CO_2 concentration (400 ppm), forests operated near carbon neutrality, with NEP periodically negative as forests shifted between operating as either carbon sink or source. Under elevated CO_2, productivity increased compared to climate-change-only simulations (Appendix Table S2, Fig. S10). CO_2 fertilization affected processes distinctly: it drove cumulative biomass increase (explaining 85% of DBH variance, 76% of AGB variance early century; Fig. 4b) but had minimal effect on annual growth rates (4% of AGB Growth variance), which were controlled primarily by water availability (49% of variance, Fig. 4b). Our CO_2 parameterization, calibrated to water-limited FACE experiments (Appendix B4), represents the saturating response observed where nutrient and hydraulic constraints limit photosynthetic enhancement (Terrer et al., 2019; Zhu et al., 2021). Uncertainty remains regarding long-term allocation responses to elevated CO_2, particularly whether sustained exposure alters carbon partitioning to roots, stems, or reproduction in ways not captured by short-term FACE experiments (Körner, 2006; Walker et al., 2021). CO_2 influenced cumulative biomass but not growth rates, suggesting that these effects operate through stand dynamics rather than accelerated individual growth. We hypothesize that CO_2-driven biomass accumulation intensified competition for water, increasing mortality of smaller trees and concentrating resources in fewer, larger individuals (Fig. S4). The resulting size class homogenization produced a forest with higher mean DBH and AGB under emission scenarios compared to current, despite lower stand density, a pattern consistent with self-thinning under resource limitation (Jiang et al., 2020). Late-century biomass projections under high CO_2 should be interpreted cautiously given allocation uncertainties.

The temporal transition from the effects of CO_2 to compound climate control is evident in driver importance (Fig. 4). Early-century responses were dominated by individual drivers (72–93% of variance), particularly CO_2 effects on structure. By late century, interactive effects accounted for 39–66% of variance, while individual CO_2 effects weakened for structural variables

https://doi.org/10.5194/egusphere-2026-2448
Preprint. Discussion started: 5 May 2026

and became non-significant for NEP and WUE. Water stress maintained consistent importance throughout (AGB growth: 49–65%, NEP: 29–49%). The dominant late-century interactions were heat stress × dry season soil moisture (11–25% across variables) and temperature × precipitation (12–25%), with CO_2 × soil moisture also prominent for NEP (20%), confirming that CO_2 benefits require adequate water and that compound stresses create non-additive effects. The scenario comparison illustrates this transition directly (Fig. 4). SSP3-7.0 produced the strongest forest response with highest biomass accumulation, WUE, and early-century productivity, because moderate CO_2 enrichment enhanced photosynthesis while climate stress remained within physiological tolerance thresholds. Under SSP5-8.5, GPP was lower than SSP3-7.0 across all periods despite CO_2 concentrations exceeding 800 ppm (Fig S8). No single climate variable explained this suppression; temperature, VPD, and water stress effects were individually weak within CO_2 levels (Figs. S9-S11). This is consistent with the dominance of compound interactive effects in the driver analysis (Fig. 4): the combined effect of higher temperatures, VPD, and reduced water availability under SSP5-8.5 suppressed photosynthetic capacity beyond what elevated CO_2 could compensate.

Mechanistically, the transition from CO_2 fertilization to water control reflects three intersecting processes evident in our simulations: (1) stomatal control initially improves WUE under elevated CO_2 but increasingly constrains carbon assimilation as VPD rises (Leuzinger and Körner, 2007; Novick et al., 2016), explaining the divergence between structural and functional responses (Fig. 3); (2) hydraulic risk reduces growth and triggers lagged mortality (Choat et al., 2018; McDowell et al., 2008), captured in our model through the hydraulic module's representation of cavitation and water potential thresholds. We observed this mechanism operating in the high-emission scenarios where CO_2 fertilization drove rapid biomass accumulation, but the maintenance respiration costs of the largest trees eventually exceeded their carbon assimilation, triggering abrupt patch-level collapse in two of five SSP5-8.5 projections (Fig. 3a.1, a.2, S8); and (3) the hydraulic module triggers drought-deciduous leaf shedding when predawn water potential falls below the turgor loss point, effectively shortening the growing season and limiting the window for CO_2 benefits (Tatarinov et al., 2016). These three mechanisms together explain why functional decline preceded structural collapse by 12-37 years and why compound climate stress progressively constrained CO_2 fertilization benefits.

4.2. Different Response Timescales for Structure Versus Function

Functional responses were more drought sensitive than structural responses. Standardized time series showed NEP was 2–3 times more sensitive to drought than AGB (Fig. S12). Similar patterns have been observed across water-limited forest systems: structural growth persisted despite declining gross primary production and net ecosystem exchange in the Mediterranean Basin (Dorado-Liñán et al., 2019), and LAI declined with increasingly variable carbon fluxes despite stable biomass in Sierra Nevada forests under future climate scenarios (Chang et al., 2025). Such analyses demonstrate that structural persistence can mask physiological stress across water-limited systems.

https://doi.org/10.5194/egusphere-2026-2448
Preprint. Discussion started: 5 May 2026

Functional physiological processes (photosynthesis, transpiration) respond within days, hours or even minutes to moisture deficits and atmospheric dryness via stomatal control, reduced carbon assimilation, and downregulated water fluxes (Adams et al., 2017). Structural stocks respond slowly because of structural inertia and physiological buffering, storage use, long turnover times and mortality lags (Anderegg et al., 2019; Hartmann et al., 2022).

Functional decline preceded structural changes by 18 ± 6 years under SSP3-7.0 and 22 ± 21 years under SSP5-8.5 (Tables S2a,b). NEP and WUE plateaued or declined by mid-century while structural variables continued increasing. Under SSP5-8.5 surviving trees grew larger in response to lower tree densities. Moreover, two of five SSP5-8.5 GCMs experienced stand-level dieback post-2080, with mean DBH dropping ~30 cm within a single year (Fig. 3a.1), indicating that physiological thresholds had been crossed. The remaining GCMs maintained biomass accumulation, masking the vulnerability revealed by earlier functional decline. The lag between functional and structural responses provides an early warning window: declining and increasingly volatile carbon uptake and water-use efficiency signal impending structural vulnerability years to decades before visible deterioration.

However, regeneration is effectively absent at Yatir. Long-term field studies report no surviving seedlings under current arid conditions (Osem et al., 2013; Pozner et al., 2022), with drought and grazing preventing recruitment (Schiller and Atzmon, 2009). ED2.2-hydraulics was initialized with observed forest inventory, effective regeneration was absent and no management interventions were simulated. Forest persistence therefore reflects survival and growth of the existing cohort only. Without recruitment, aging forests face a demographic trap where biomass accumulates but declining functional capacity hides vulnerability and threatens long-term persistence.

4.3. Management and Monitoring in a Shifting Climate

Structural responses alone mask early stress. While AGB may remain stable or even increase under mounting stress, functional responses and LAI, decline much earlier, providing a window of 1-4 decades for intervention. LAI decline appears particularly valuable as an early-warning indicator of climate vulnerability, preceding biomass loss by decades in our dryland pine forest as well as in Sierra Nevada predictions (Chang et al., 2025). Detecting functional decline requires monitoring tools sensitive to physiological stress, such as satellite-derived LAI, eddy covariance flux measurements, solar-induced fluorescence (Yang et al., 2015) rather than structural inventories alone.

Our simulations also reveal a demographic trap: functional decline combined with a complete absence of regeneration means that high biomass stocks provide only temporary stability. Once the aging cohort declines, losses may be abrupt (De Kauwe et al., 2014). The apparent paradox of increasing AGB alongside declining stem density illustrates why structural metrics can mislead: coarse inventory or remote-sensing estimates of total AGB can mask the absence of recruitment, misrepresenting forest health until surviving individuals succumb. The LAI recovery following mortality events in our simulations suggests

https://doi.org/10.5194/egusphere-2026-2448
Preprint. Discussion started: 5 May 2026

that density reduction can temporarily restore canopy function, consistent with experimental thinning results in dryland *P. halepensis* plantations showing improved growth, reduced drought sensitivity, and lower mortality (Calev et al., 2016). Adaptive thinning may therefore extend forest longevity under increasing drought, though it cannot substitute for regeneration. While fire disturbance was not simulated due to active suppression at Yatir, fuel accumulation for wildfires under increasing climatic stress raises additional risk of abrupt carbon release (Steel et al., 2015). Long-term forest persistence requires species that combine drought tolerance, regeneration capacity, fire resilience, and complementary functional traits (Hisano et al., 2024; Irob et al., 2023).

Although this study focused on a single planted forest, Yatir, its lessons extend to other afforestation projects in Mediterranean, subtropical, arid and semiarid zones facing similar constraints. Afforestation remains an important climate-mitigation tool, but continued growth of surviving trees can mask progressive stand thinning, giving a false sense of permanence. Our results question the long-term viability of dryland afforestation without adaptive management and emphasize that studies promoting large-scale dryland planting initiatives (Bastin et al., 2019) overlook these critical constraints. Integrating functional monitoring with process-based modeling offers the clearest path for detecting vulnerability and guiding adaptive management.

4.4. Model Performance and Limitations in Dryland Forests

ED2.2 with hydraulics reproduced structural growth, seasonal fluxes, and drought responses in an extreme dryland system with modest adjustments. Accurate simulation required matching carbon and water fluxes, LAI, and biomass simultaneously (Feng et al., 2018; Zhang et al., 2022); calibration to GPP alone was insufficient (Pandit et al., 2019). Proper model initialization with observed ecosystem structure was critical, since initialization effects can persist for decades (Chang et al., 2025).

However, as with any model, limitations remain and affect the interpretation of model predictions in specific ways. The model underestimated ecosystem respiration, with the largest discrepancies during the wet season. The simplified decomposition module lacks photodegradation and post-rainfall pulse dynamics that dominate dryland carbon cycling (Grünzweig et al., 2022), and insufficient soil carbon substrate from the historical spin-up may further reduce heterotrophic respiration. Together, these likely cause projected NEP to be high. Carbon fluxes peak in spring, when soil moisture is adequate, temperature rises, and low VPD levels simultaneously relax environmental constraints. Our model underestimates this spring peak, likely reflecting fixed physiological parameters that cannot reproduce such nonlinear responses, a limitation also reported in other ED2.2 applications to dryland systems (Dashti et al., 2021; Pandit et al., 2018), resulting in a potential underestimation of early-century CO_2 fertilization benefits. The muted summer LAI reduction indicates that the evergreen phenology module underestimates seasonal drought response of *P. halepensis*. The hydraulic module's leaf shedding mechanism provides insufficient adjustment under moderate water stress, potentially delaying projected functional decline. The model also lacks hydraulic redistribution, which may overestimate shallow-soil drought stress. CO_2 fertilization was constrained based on FACE experiments and limited by the hydraulic module's water stress response, producing realistic elevated CO_2 responses under

https://doi.org/10.5194/egusphere-2026-2448
Preprint. Discussion started: 5 May 2026

water limitation, though projections may be slightly optimistic given uncertainties in nutrient constraints. Future improvements of the model should include the implementation of mechanistic nutrient-water cycling, photodegradation, hydraulic redistribution and formal optimization frameworks that maintain ecological constraints while efficiently exploring parameter uncertainty.

Despite these limitations, the model captured core dryland forest dynamics, highlighting its potential for evaluating afforestation strategies and ecosystem resilience under climate change.

5. Conclusion

Our study demonstrated that the responses of dryland afforestation systems are not static but evolve with climate trajectories: early gains from CO_2 fertilization give way to water limitation and heat stress, resulting in increasing volatility and declines in forest functioning. Under the highest emission scenario, compound climate stress suppressed productivity below the moderate-emission scenario despite higher CO_2, confirming that fertilization benefits cannot compensate for the extremes they accompany. In *P. halepensis*, drought tolerance has allowed growth to persist under increasingly arid conditions, but productivity and water-use efficiency declined earlier, with functional responses preceding structural decline. This lag reveals a demographic trap in which aging cohorts mask emerging forest vulnerability.

These findings emphasize that traditional forest surveys cannot serve alone as indicators of forest health. Instead, functional monitoring is essential for detecting vulnerability early and sustaining forest services under accelerating climate change.

Beyond Yatir, our results highlight a broader principle: afforestation projects at the dry margin of forest viability may provide only temporary carbon sinks. Models such as ED2.2-hydraulics, when calibrated to multiple functional and structural responses, can help anticipate these temporal shifts and guide climate policy. Ensuring the long-term contribution of forests to climate mitigation requires embracing their dynamic nature, acknowledging that resilience today does not guarantee persistence tomorrow.

Acknowledgments

The authors would like to thank the Hebrew University Research Computing Service (HURCS) for their support. K.I. gratefully acknowledges the Azrieli Foundation for support through an Azrieli Fellowship. We thank Paul Moorcroft for his insightful input on this study, Dan Yakir for the Yatir eddy covariance flux tower data and Tamir Klein for provision of validation data. For their roles in producing, coordinating, and making the ISIMIP input data available, we acknowledge the ISIMIP cross-sectoral science team. This work was funded by the Ministry of Environmental Protection within the framework of the #22-1-17 project. We used OpenAI's ChatGPT to support writing refinement and language editing, as well as to help synthesize the literature. All content was subsequently reviewed, verified, and edited by the authors to ensure scientific accuracy and integrity. We used Anthropic's Claude AI (accessed in 2025) to assist in drafting R scripts for figure generation and to support parts of

https://doi.org/10.5194/egusphere-2026-2448
Preprint. Discussion started: 5 May 2026

the model calibration process, specifically for code generation and identifying key parameter–process linkages in ED2.2. All scripts and analytical decisions were critically reviewed, tested, and validated by the authors to ensure scientific integrity and reproducibility.

Conflict of Interest Statement

The authors have no conflicts of interest to declare.

Author Contributions

Katja Irob: Conceptualization, Methodology, Software, Formal analysis, Visualization, Writing - Original draft preparation. **Efrat Sheffer**: Conceptualization, Writing - Reviewing and Editing, Supervision. **José Grünzweig**: Conceptualization, Writing - Reviewing and Editing, Supervision. **Yakir Preisler**: Conceptualization, Methodology. **Liling Chang**: Conceptualization, Methodology, Writing - Reviewing and Editing. **Sebastian Fiedler**: Software, Validation, Writing - Reviewing and Editing. **Matthias Büchner**: Data curation, Resources.

Open Research Statement

Model code, simulation data and scripts to reproduce the results and figures of this manuscript will be made available upon publication via the FigShare Digital Repository and can be accessed via this private link during the review process: https://figshare.com/s/ba35aadfb4dfa9606f53. The original and current versions of the ED2.2 model are openly accessible on GitHub at https://github.com/EDmodel/ED2, where it is actively maintained and regularly updated by the repository developers.

References

Adams, H. D., Guardiola-Claramonte, M., Barron-Gafford, G. A., Villegas, J. C., Breshears, D. D., Zou, C. B., Troch, P. A., and Huxman, T. E.: Temperature sensitivity of drought-induced tree mortality portends increased regional die-off under global-change-type drought, Proc. Natl. Acad. Sci., 106, 7063–7066, https://doi.org/10.1073/pnas.0901438106, 2009.

Adams, H. D., Zeppel, M. J. B., Anderegg, W. R. L., Hartmann, H., Landhäusser, S. M., Tissue, D. T., Huxman, T. E., Hudson, P. J., Franz, T. E., Allen, C. D., Anderegg, L. D. L., Barron-Gafford, G. A., Beerling, D. J., Breshears, D. D., Brodribb, T. J., Bugmann, H., Cobb, R. C., Collins, A. D., Dickman, L. T., Duan, H., Ewers, B. E., Galiano, L., Galvez, D. A., Garcia-Forner, N., Gaylord, M. L., Germino, M. J., Gessler, A., Hacke, U. G., Hakamada, R., Hector, A., Jenkins, M. W., Kane, J. M., Kolb, T. E., Law, D. J., Lewis, J. D., Limousin, J.-M., Love, D. M., Macalady, A. K., Martínez-Vilalta, J., Mencuccini, M., Mitchell, P. J., Muss, J. D., O'Brien, M. J., O'Grady, A. P., Pangle, R. E., Pinkard, E. A., Piper, F. I., Plaut, J. A., Pockman, W. T., Quirk, J., Reinhardt, K., Ripullone, F., Ryan, M. G., Sala, A., Sevanto, S., Sperry, J. S., Vargas, R., Vennetier, M., Way, D.

https://doi.org/10.5194/egusphere-2026-2448
Preprint. Discussion started: 5 May 2026

A., Xu, C., Yepez, E. A., and McDowell, N. G.: A multi-species synthesis of physiological mechanisms in drought-induced tree mortality, Nat. Ecol. Evol., 1, 1285–1291, https://doi.org/10.1038/s41559-017-0248-x, 2017.

Ahlström, A., Raupach, M. R., Schurgers, G., Smith, B., Arneth, A., Jung, M., Reichstein, M., Canadell, J. G., Friedlingstein, P., Jain, A. K., Kato, E., Poulter, B., Sitch, S., Stocker, B. D., Viovy, N., Wang, Y. P., Wiltshire, A., Zaehle, S., and Zeng, N.: The dominant role of semi-arid ecosystems in the trend and variability of the land CO2 sink, Science, 348, 895–899, https://doi.org/10.1126/science.aaa1668, 2015.

Anderegg, W. R. L., Trugman, A. T., Bowling, D. R., Salvucci, G., and Tuttle, S. E.: Plant functional traits and climate influence drought intensification and land–atmosphere feedbacks, Proc. Natl. Acad. Sci., 116, 14071–14076, https://doi.org/10.1073/pnas.1904747116, 2019.

Anderegg, W. R. L., Trugman, A. T., Badgley, G., Anderson, C. M., Bartuska, A., Ciais, P., Cullenward, D., Field, C. B., Freeman, J., Goetz, S. J., Hicke, J. A., Huntzinger, D., Jackson, R. B., Nickerson, J., Pacala, S., and Randerson, J. T.: Climate-driven risks to the climate mitigation potential of forests, Science, 368, eaaz7005, https://doi.org/10.1126/science.aaz7005, 2020.

Antonarakis, A. S., Bogan, S. A., Goulden, M. L., and Moorcroft, P. R.: Impacts of the 2012–2015 Californian drought on carbon, water and energy fluxes in the Californian Sierras: Results from an imaging spectrometry-constrained terrestrial biosphere model, Glob. Change Biol., 28, 1823–1852, https://doi.org/10.1111/gcb.15995, 2022.

Bastin, J.-F., Finegold, Y., Garcia, C., Mollicone, D., Rezende, M., Routh, D., Zohner, C. M., and Crowther, T. W.: The global tree restoration potential, Science, 365, 76–79, https://doi.org/10.1126/science.aax0848, 2019.

Cai, J.: humidity: Calculate Water Vapor Measures from Temperature and Dew Point, 2019.

Calev, A., Zoref, C., Tzukerman, M., Moshe, Y., Zangy, E., and Osem, Y.: High-intensity thinning treatments in mature Pinus halepensis plantations experiencing prolonged drought, Eur. J. For. Res., 135, 551–563, https://doi.org/10.1007/s10342-016-0954-y, 2016.

Chang, L.-L., Liu, S., Antonarakis, A. S., Longo, M., Tang, H., Armston, J. D., Dubayah, R., and Moorcroft, P.: Legacies of model initialization on predictions of future ecosystem dynamics in California's Sierra Nevada: insights from GEDI, New Phytol., 248, 2809–2832, https://doi.org/10.1111/nph.70657, 2025.

Choat, B., Brodribb, T. J., Brodersen, C. R., Duursma, R. A., López, R., and Medlyn, B. E.: Triggers of tree mortality under drought, Nature, 558, 531–539, https://doi.org/10.1038/s41586-018-0240-x, 2018.

Cos, J., Doblas-Reyes, F., Jury, M., Marcos, R., Bretonnière, P.-A., and Samsó, M.: The Mediterranean climate change hotspot in the CMIP5 and CMIP6 projections, Earth Syst. Dyn., 13, 321–340, https://doi.org/10.5194/esd-13-321-2022, 2022.

Dashti, H., Pandit, K., Glenn, N. F., Shinneman, D. J., Flerchinger, G. N., Hudak, A. T., de Graaf, M. A., Flores, A., Ustin, S., Ilangakoon, N., and Fellows, A. W.: Performance of the ecosystem demography model (EDv2.2) in simulating gross primary production capacity and activity in a dryland study area, Agric. For. Meteorol., 297, 108270, https://doi.org/10.1016/j.agrformet.2020.108270, 2021.

De Kauwe, M. G., Medlyn, B. E., Zaehle, S., Walker, A. P., Dietze, M. C., Wang, Y.-P., Luo, Y., Jain, A. K., El-Masri, B., Hickler, T., Wårlind, D., Weng, E., Parton, W. J., Thornton, P. E., Wang, S., Prentice, I. C., Asao, S., Smith, B., McCarthy, H. R., Iversen, C. M., Hanson, P. J., Warren, J. M., Oren, R., and Norby, R. J.: Where does the carbon go? A model–data intercomparison of vegetation carbon allocation and turnover processes at two temperate forest free-air CO2 enrichment sites, New Phytol., 203, 883–899, https://doi.org/10.1111/nph.12847, 2014.

https://doi.org/10.5194/egusphere-2026-2448
Preprint. Discussion started: 5 May 2026

Dorado-Liñán, I., Piovesan, G., Martínez-Sancho, E., Gea-Izquierdo, G., Zang, C., Cañellas, I., Castagneri, D., Di Filippo, A., Gutiérrez, E., Ewald, J., Fernández-de-Uña, L., Hornstein, D., Jantsch, M. C., Levanič, T., Mellert, K. H., Vacchiano, G., Zlatanov, T., and Menzel, A.: Geographical adaptation prevails over species-specific determinism in trees' vulnerability to climate change at Mediterranean rear-edge forests, Glob. Change Biol., 25, 1296–1314, https://doi.org/10.1111/gcb.14544, 2019.

Dorman, M., Perevolotsky, A., Sarris, D., and Svoray, T.: The effect of rainfall and competition intensity on forest response to drought: lessons learned from a dry extreme, Oecologia, 177, 1025–1038, https://doi.org/10.1007/s00442-015-3229-2, 2015.

Drori, R., Ziv, B., Saaroni, H., Etkin, A., and Sheffer, E.: Recent changes in the rain regime over the Mediterranean climate region of Israel, Clim. Change, 167, 15, https://doi.org/10.1007/s10584-021-03161-6, 2021.

Fatichi, S., Pappas, C., Zscheischler, J., and Leuzinger, S.: Modelling carbon sources and sinks in terrestrial vegetation, New Phytol., 221, 652–668, https://doi.org/10.1111/nph.15451, 2019.

Feng, X., Uriarte, M., González, G., Reed, S., Thompson, J., Zimmerman, J. K., and Murphy, L.: Improving predictions of tropical forest response to climate change through integration of field studies and ecosystem modeling, Glob. Change Biol., 24, e213–e232, https://doi.org/10.1111/gcb.13863, 2018.

Friedlingstein, P., Allen, M., Canadell, J. G., Peters, G. P., and Seneviratne, S. I.: Comment on "The global tree restoration potential," Science, 366, eaay8060, https://doi.org/10.1126/science.aay8060, 2019.

Friedlingstein, P., O'Sullivan, M., Jones, M. W., Andrew, R. M., Gregor, L., Hauck, J., Le Quéré, C., Luijkx, I. T., Olsen, A., Peters, G. P., Peters, W., Pongratz, J., Schwingshackl, C., Sitch, S., Canadell, J. G., Ciais, P., Jackson, R. B., Alin, S. R., Alkama, R., Arneth, A., Arora, V. K., Bates, N. R., Becker, M., Bellouin, N., Bittig, H. C., Bopp, L., Chevallier, F., Chini, L. P., Cronin, M., Evans, W., Falk, S., Feely, R. A., Gasser, T., Gehlen, M., Gkritzalis, T., Gloege, L., Grassi, G., Gruber, N., Gürses, Ö., Harris, I., Hefner, M., Houghton, R. A., Hurtt, G. C., Iida, Y., Ilyina, T., Jain, A. K., Jersild, A., Kadono, K., Kato, E., Kennedy, D., Klein Goldewijk, K., Knauer, J., Korsbakken, J. I., Landschützer, P., Lefèvre, N., Lindsay, K., Liu, J., Liu, Z., Marland, G., Mayot, N., McGrath, M. J., Metzl, N., Monacci, N. M., Munro, D. R., Nakaoka, S.-I., Niwa, Y., O'Brien, K., Ono, T., Palmer, P. I., Pan, N., Pierrot, D., Pocock, K., Poulter, B., Resplandy, L., Robertson, E., Rödenbeck, C., Rodriguez, C., Rosan, T. M., Schwinger, J., Séférian, R., Shutler, J. D., Skjelvan, I., Steinhoff, T., Sun, Q., Sutton, A. J., Sweeney, C., Takao, S., Tanhua, T., Tans, P. P., Tian, X., Tian, H., Tilbrook, B., Tsujino, H., Tubiello, F., van der Werf, G. R., Walker, A. P., Wanninkhof, R., Whitehead, C., Willstrand Wranne, A., et al.: Global Carbon Budget 2022, Earth Syst. Sci. Data, 14, 4811–4900, https://doi.org/10.5194/essd-14-4811-2022, 2022.

Gebrechorkos, S., Leyland, J., Slater, L., Wortmann, M., Ashworth, P. J., Bennett, G. L., Boothroyd, R., Cloke, H., Delorme, P., Griffith, H., Hardy, R., Hawker, L., McLelland, S., Neal, J., Nicholas, A., Tatem, A. J., Vahidi, E., Parsons, D. R., and Darby, S. E.: A high-resolution daily global dataset of statistically downscaled CMIP6 models for climate impact analyses, Sci. Data, 10, 611, https://doi.org/10.1038/s41597-023-02528-x, 2023.

Grünzweig, J. M., Lin, T., Rotenberg, E., Schwartz, A., and Yakir, D.: Carbon sequestration in arid-land forest, Glob. Change Biol., 9, 791–799, https://doi.org/10.1046/j.1365-2486.2003.00612.x, 2003.

Grünzweig, J. M., De Boeck, H. J., Rey, A., Santos, M. J., Adam, O., Bahn, M., Belnap, J., Deckmyn, G., Dekker, S. C., Flores, O., Gliksman, D., Helman, D., Hultine, K. R., Liu, L., Meron, E., Michael, Y., Sheffer, E., Throop, H. L., Tzuk, O., and Yakir, D.: Dryland mechanisms could widely control ecosystem functioning in a drier and warmer world, Nat. Ecol. Evol., 6, 1064–1076, https://doi.org/10.1038/s41559-022-01779-y, 2022.

Hartmann, H., Bastos, A., Das, A. J., Esquivel-Muelbert, A., Hammond, W. M., Martínez-Vilalta, J., McDowell, N. G., Powers, J. S., Pugh, T. A. M., Ruthrof, K. X., and Allen, C. D.: Climate Change Risks to Global Forest Health: Emergence of

https://doi.org/10.5194/egusphere-2026-2448
Preprint. Discussion started: 5 May 2026

Unexpected Events of Elevated Tree Mortality Worldwide, Annu. Rev. Plant Biol., 73, 673–702, https://doi.org/10.1146/annurev-arplant-102820-012804, 2022.

Hisano, M., Ghazoul, J., Chen, X., and Chen, H. Y. H.: Functional diversity enhances dryland forest productivity under long-term climate change, Sci. Adv., 10, eadn4152, https://doi.org/10.1126/sciadv.adn4152, 2024.

Huang, X., Zhen ,Zhen, Zhao ,Wenxin, and and Wang, X.: Forest carbon sink in North China increased in recent two decades, but decreased in extreme drought years, GIScience Remote Sens., 61, 2383040, https://doi.org/10.1080/15481603.2024.2383040, 2024.

IPCC: Climate Change 2022: Impacts, Adaptation, and Vulnerability., 2022.

Irob, K., Blaum, N., Weiss-Aparicio, A., Hauptfleisch, M., Hering, R., Uiseb, K., and Tietjen, B.: Savanna resilience to droughts increases with the proportion of browsing wild herbivores and plant functional diversity, J. Appl. Ecol., 60, 251–262, https://doi.org/10.1111/1365-2664.14351, 2023.

Jiang, M., Medlyn, B. E., Drake, J. E., Duursma, R. A., Anderson, I. C., Barton, C. V. M., Boer, M. M., Carrillo, Y., Castañeda-Gómez, L., Collins, L., Crous, K. Y., De Kauwe, M. G., dos Santos, B. M., Emmerson, K. M., Facey, S. L., Gherlenda, A. N., Gimeno, T. E., Hasegawa, S., Johnson, S. N., Kännaste, A., Macdonald, C. A., Mahmud, K., Moore, B. D., Nazaries, L., Neilson, E. H. J., Nielsen, U. N., Niinemets, Ü., Noh, N. J., Ochoa-Hueso, R., Pathare, V. S., Pendall, E., Pihlblad, J., Piñeiro, J., Powell, J. R., Power, S. A., Reich, P. B., Renchon, A. A., Riegler, M., Rinnan, R., Rymer, P. D., Salomón, R. L., Singh, B. K., Smith, B., Tjoelker, M. G., Walker, J. K. M., Wujeska-Klause, A., Yang, J., Zaehle, S., and Ellsworth, D. S.: The fate of carbon in a mature forest under carbon dioxide enrichment, Nature, 580, 227–231, https://doi.org/10.1038/s41586-020-2128-9, 2020.

Johnston, M.: Plant temperature in a Mediterranean woodland savanna: Measurements and models, 2021.

Kannenberg, S. A., Schwalm, C. R., and Anderegg, W. R. L.: Ghosts of the past: how drought legacy effects shape forest functioning and carbon cycling, Ecol. Lett., 23, 891–901, https://doi.org/10.1111/ele.13485, 2020.

Klein, T., Cohen, S., and Yakir, D.: Hydraulic adjustments underlying drought resistance of Pinus halepensis, Tree Physiol., 31, 637–648, https://doi.org/10.1093/treephys/tpr047, 2011.

Klein, T., Rotenberg, E., Cohen-Hilaleh, E., Raz-Yaseef, N., Tatarinov, F., Preisler, Y., Ogée, J., Cohen, S., and Yakir, D.: Quantifying transpirable soil water and its relations to tree water use dynamics in a water-limited pine forest, Ecohydrology, 7, 409–419, https://doi.org/10.1002/eco.1360, 2014.

Körner, C.: Plant CO2 responses: an issue of definition, time and resource supply, New Phytol., 172, 393–411, https://doi.org/10.1111/j.1469-8137.2006.01886.x, 2006.

Lange, S. and Büchner, M.: ISIMIP3b bias-adjusted atmospheric climate input data (v1.1), https://doi.org/10.48364/ISIMIP.842396.1, 2021.

Leuzinger, S. and Körner, C.: Water savings in mature deciduous forest trees under elevated CO2, Glob. Change Biol., 13, 2498–2508, https://doi.org/10.1111/j.1365-2486.2007.01467.x, 2007.

Longo, M., Knox, R. G., Medvigy, D. M., Levine, N. M., Dietze, M. C., Kim, Y., Swann, A. L. S., Zhang, K., Rollinson, C. R., Bras, R. L., Wofsy, S. C., and Moorcroft, P. R.: The biophysics, ecology, and biogeochemistry of functionally diverse, vertically and horizontally heterogeneous ecosystems: the Ecosystem Demography model, version 2.2 – Part 1: Model description, Geosci. Model Dev., 12, 4309–4346, https://doi.org/10.5194/gmd-12-4309-2019, 2019.

https://doi.org/10.5194/egusphere-2026-2448
Preprint. Discussion started: 5 May 2026

McDowell, N., Pockman, W. T., Allen, C. D., Breshears, D. D., Cobb, N., Kolb, T., Plaut, J., Sperry, J., West, A., Williams, D. G., and Yepez, E. A.: Mechanisms of plant survival and mortality during drought: why do some plants survive while others succumb to drought?, New Phytol., 178, 719–739, https://doi.org/10.1111/j.1469-8137.2008.02436.x, 2008.

McDowell, N. G., Allen, C. D., Anderson-Teixeira, K., Aukema, B. H., Bond-Lamberty, B., Chini, L., Clark, J. S., Dietze, M., Grossiord, C., Hanbury-Brown, A., Hurtt, G. C., Jackson, R. B., Johnson, D. J., Kueppers, L., Lichstein, J. W., Ogle, K., Poulter, B., Pugh, T. A. M., Seidl, R., Turner, M. G., Uriarte, M., Walker, A. P., and Xu, C.: Pervasive shifts in forest dynamics in a changing world, Science, 368, eaaz9463, https://doi.org/10.1126/science.aaz9463, 2020.

Moorcroft, P. R., Hurtt, G. C., and Pacala, S. W.: A method for scaling vegetation dynamics: the ecosystem demography model (ED), Ecol. Monogr., 71, 557–586, 2001.

Morán-Ordóñez, A., Ramsauer, J., Coll, L., Brotons, L., and Ameztegui, A.: Ecosystem services provision by Mediterranean forests will be compromised above 2°C warming, Glob. Change Biol., 27, 4210–4222, https://doi.org/10.1111/gcb.15745, 2021.

Novick, K. A., Ficklin, D. L., Stoy, P. C., Williams, C. A., Bohrer, G., Oishi, A. C., Papuga, S. A., Blanken, P. D., Noormets, A., Sulman, B. N., Scott, R. L., Wang, L., and Phillips, R. P.: The increasing importance of atmospheric demand for ecosystem water and carbon fluxes, Nat. Clim. Change, 6, 1023–1027, https://doi.org/10.1038/nclimate3114, 2016.

Ogaya, R. and Peñuelas, J.: Climate Change Effects in a Mediterranean Forest Following 21 Consecutive Years of Experimental Drought, Forests, 12, 306, https://doi.org/10.3390/f12030306, 2021.

Osem, Y., Yavlovich, H., Zecharia, N., Atzmon, N., Moshe, Y., and Schiller, G.: Fire-free natural regeneration in water limited Pinus halepensis forests: a silvicultural approach, Eur. J. For. Res., 132, 679–690, https://doi.org/10.1007/s10342-013-0704-3, 2013.

Pandit, K., Dashti, H., Glenn, N. F., Flores, A. N., Maguire, K. C., Shinneman, D. J., Flerchinger, G. N., and Fellows, A. W.: Optimizing shrub parameters to estimate gross primary production of the sagebrush ecosystem using the Ecosystem Demography (EDv2.2) model, https://doi.org/10.5194/gmd-2018-264, 13 December 2018.

Pandit, K., Dashti, H., Glenn, N. F., Flores, A. N., Maguire, K. C., Shinneman, D. J., Flerchinger, G. N., and Fellows, A. W.: Developing and optimizing shrub parameters representing sagebrush (*Artemisia* spp.) ecosystems in the northern Great Basin using the Ecosystem Demography (EDv2.2) model, Geosci. Model Dev., 12, 4585–4601, https://doi.org/10.5194/gmd-12-4585-2019, 2019.

Peñuelas, J., Ciais, P., Canadell, J. G., Janssens, I. A., Fernández-Martínez, M., Carnicer, J., Obersteiner, M., Piao, S., Vautard, R., and Sardans, J.: Shifting from a fertilization-dominated to a warming-dominated period, Nat. Ecol. Evol., 1, 1438–1445, https://doi.org/10.1038/s41559-017-0274-8, 2017.

Pozner, E., Bar-On, P., Livne-Luzon, S., Moran, U., Tsamir-Rimon, M., Dener, E., Schwartz, E., Rotenberg, E., Tatarinov, F., Preisler, Y., Zecharia, N., Osem, Y., Yakir, D., and Klein, T.: A hidden mechanism of forest loss under climate change: The role of drought in eliminating forest regeneration at the edge of its distribution, For. Ecol. Manag., 506, 119966, https://doi.org/10.1016/j.foreco.2021.119966, 2022.

Preisler, Y., Tatarinov, F., Grünzweig, J. M., Bert, D., Ogée, J., Wingate, L., Rotenberg, E., Rohatyn, S., Her, N., Moshe, I., Klein, T., and Yakir, D.: Mortality versus survival in drought-affected Aleppo pine forest depends on the extent of rock cover and soil stoniness, Funct. Ecol., 33, 901–912, https://doi.org/10.1111/1365-2435.13302, 2019.

https://doi.org/10.5194/egusphere-2026-2448
Preprint. Discussion started: 5 May 2026

Preisler, Y., Tatarinov, F., Grünzweig, J. M., and Yakir, D.: Seeking the "point of no return" in the sequence of events leading to mortality of mature trees, Plant Cell Environ., 44, 1315–1328, https://doi.org/10.1111/pce.13942, 2021.

R Core Team: R: A Language and Environment for Statistical Computing, 2025.

Reichstein, M., Bahn, M., Ciais, P., Frank, D., Mahecha, M. D., Seneviratne, S. I., Zscheischler, J., Beer, C., Buchmann, N., Frank, D. C., Papale, D., Rammig, A., Smith, P., Thonicke, K., van der Velde, M., Vicca, S., Walz, A., and Wattenbach, M.: Climate extremes and the carbon cycle, Nature, 500, 287–295, https://doi.org/10.1038/nature12350, 2013.

Rohatyn, S., Yakir, D., Rotenberg, E., and Carmel, Y.: Limited climate change mitigation potential through forestation of the vast dryland regions, Science, 377, 1436–1439, https://doi.org/10.1126/science.abm9684, 2022.

Ruehr, S., Keenan, T. F., Williams, C., Zhou, Y., Lu, X., Bastos, A., Canadell, J. G., Prentice, I. C., Sitch, S., and Terrer, C.: Evidence and attribution of the enhanced land carbon sink, Nat. Rev. Earth Environ., 4, 518–534, https://doi.org/10.1038/s43017-023-00456-3, 2023.

Schiller, G. and Atzmon, N.: Performance of Aleppo pine (*Pinus halepensis*) provenances grown at the edge of the Negev desert: A review, J. Arid Environ., 73, 1051–1057, https://doi.org/10.1016/j.jaridenv.2009.06.003, 2009.

Shekhar, A., Hörtnagl, L., Paul-Limoges, E., Etzold, S., Zweifel, R., Buchmann, N., and Gharun, M.: Contrasting impact of extreme soil and atmospheric dryness on the functioning of trees and forests, Sci. Total Environ., 916, 169931, https://doi.org/10.1016/j.scitotenv.2024.169931, 2024.

Sprintsin, M., Cohen, S., Maseyk, K., Rotenberg, E., Grünzweig, J., Karnieli, A., Berliner, P., and Yakir, D.: Long term and seasonal courses of leaf area index in a semi-arid forest plantation, Agric. For. Meteorol., 151, 565–574, https://doi.org/10.1016/j.agrformet.2011.01.001, 2011.

Steel, Z. L., Safford, H. D., and Viers, J. H.: The fire frequency-severity relationship and the legacy of fire suppression in California forests, Ecosphere, 6, art8, https://doi.org/10.1890/ES14-00224.1, 2015.

Tatarinov, F., Rotenberg, E., Maseyk, K., Ogée, J., Klein, T., and Yakir, D.: Resilience to seasonal heat wave episodes in a Mediterranean pine forest, New Phytol., 210, 485–496, https://doi.org/10.1111/nph.13791, 2016.

Terrer, C., Jackson, R. B., Prentice, I. C., Keenan, T. F., Kaiser, C., Vicca, S., Fisher, J. B., Reich, P. B., Stocker, B. D., Hungate, B. A., Peñuelas, J., McCallum, I., Soudzilovskaia, N. A., Cernusak, L. A., Talhelm, A. F., Van Sundert, K., Piao, S., Newton, P. C. D., Hovenden, M. J., Blumenthal, D. M., Liu, Y. Y., Müller, C., Winter, K., Field, C. B., Viechtbauer, W., Van Lissa, C. J., Hoosbeek, M. R., Watanabe, M., Koike, T., Leshyk, V. O., Polley, H. W., and Franklin, O.: Nitrogen and phosphorus constrain the CO2 fertilization of global plant biomass, Nat. Clim. Change, 9, 684–689, https://doi.org/10.1038/s41558-019-0545-2, 2019.

Väänänen, P. J., Osem, Y., Cohen, S., and Grünzweig, J. M.: Differential drought resistance strategies of co-existing woodland species enduring the long rainless Eastern Mediterranean summer, Tree Physiol., 40, 305–320, https://doi.org/10.1093/treephys/tpz130, 2020.

Walker, A. P., De Kauwe, M. G., Bastos, A., Belmecheri, S., Georgiou, K., Keeling, R. F., McMahon, S. M., Medlyn, B. E., Moore, D. J. P., Norby, R. J., Zaehle, S., Anderson-Teixeira, K. J., Battipaglia, G., Brienen, R. J. W., Cabugao, K. G., Cailleret, M., Campbell, E., Canadell, J. G., Ciais, P., Craig, M. E., Ellsworth, D. S., Farquhar, G. D., Fatichi, S., Fisher, J. B., Frank, D. C., Graven, H., Gu, L., Haverd, V., Heilman, K., Heimann, M., Hungate, B. A., Iversen, C. M., Joos, F., Jiang, M., Keenan, T. F., Knauer, J., Körner, C., Leshyk, V. O., Leuzinger, S., Liu, Y., MacBean, N., Malhi, Y., McVicar, T. R., Penuelas, J., Pongratz, J., Powell, A. S., Riutta, T., Sabot, M. E. B., Schleucher, J., Sitch, S., Smith, W. K., Sulman, B., Taylor, B., Terrer,

https://doi.org/10.5194/egusphere-2026-2448
Preprint. Discussion started: 5 May 2026

751 C., Torn, M. S., Treseder, K. K., Trugman, A. T., Trumbore, S. E., van Mantgem, P. J., Voelker, S. L., Whelan, M. E., and
752 Zuidema, P. A.: Integrating the evidence for a terrestrial carbon sink caused by increasing atmospheric CO2, New Phytol.,
753 229, 2413–2445, https://doi.org/10.1111/nph.16866, 2021.

754 Wood, S. N.: Generalized Additive Models: An Introduction with R (2nd ed.)., 2017.

755 Xu, X., Medvigy, D., Powers, J. S., Becknell, J. M., and Guan, K.: Diversity in plant hydraulic traits explains seasonal and
756 inter-annual variations of vegetation dynamics in seasonally dry tropical forests, New Phytol., 212, 80–95,
757 https://doi.org/10.1111/nph.14009, 2016.

758 Yang, X., Tang, J., Mustard, J. F., Lee, J.-E., Rossini, M., Joiner, J., Munger, J. W., Kornfeld, A., and Richardson, A. D.:
759 Solar-induced chlorophyll fluorescence that correlates with canopy photosynthesis on diurnal and seasonal scales in a
760 temperate deciduous forest, Geophys. Res. Lett., 42, 2977–2987, https://doi.org/10.1002/2015GL063201, 2015.

761 Yosef, G., Walko, R., Avisar, R., Tatarinov, F., Rotenberg, E., and Yakir, D.: Large-scale semi-arid afforestation can enhance
762 precipitation and carbon sequestration potential, Sci. Rep., 8, 996, https://doi.org/10.1038/s41598-018-19265-6, 2018.

763 Zhang, J., Bras, R. L., Longo, M., and Heartsill Scalley, T.: The impact of hurricane disturbances on a tropical forest:
764 implementing a palm plant functional type and hurricane disturbance module in ED2-HuDi V1.0, Geosci. Model Dev., 15,
765 5107–5126, https://doi.org/10.5194/gmd-15-5107-2022, 2022.

766 Zhu, Z., Zeng, H., Myneni, R. B., Chen, C., Zhao, Q., Zha, J., Zhan, S., and MacLachlan, I.: Comment on “Recent global
767 decline of CO2 fertilization effects on vegetation photosynthesis,” Science, 373, eabg5673,
768 https://doi.org/10.1126/science.abg5673, 2021.

769

770